Synthesis and Reactivity in Inorganic, Metal-Organic, and Nano-Metal Chemistry

ISSN: 1553-3174 (Print) 1553-3182 (Online) Journal homepage: www.tandfonline.com/journals/lsrt20

Preparation of PVP (Polyvinyl Pyrrolidone)/Ba-Sr Hexaferrites via Gel to Crystalline Method

Z. Durmus, A. Baykal, H. Sozeri & M. S. Toprak

To cite this article: Z. Durmus, A. Baykal, H. Sozeri & M. S. Toprak (2012) Preparation of PVP (Polyvinyl Pyrrolidone)/Ba-Sr Hexaferrites via Gel to Crystalline Method, Synthesis and Reactivity in Inorganic, Metal-Organic, and Nano-Metal Chemistry, 42:10, 1390-1397, DOI: 10.1080/15533174.2012.680150

To link to this article: https://doi.org/10.1080/15533174.2012.680150

Synthesis and Reactivity in Inorganic, Metal-Organic, and Nano-Metal Chemistry, 42:1390–1397, 2012
Copyright © Taylor & Francis Group, LLC
ISSN: 1553-3174 print / 1553-3182 online
DOI: 10.1080/15533174.2012.680150

Preparation of PVP (Polyvinyl Pyrrolidone)/Ba-Sr Hexaferrites via Gel to Crystalline Method

Z. Durmus,[1] A. Baykal,[1] H. Sozeri,[2] and M. S. Toprak[3,4]
[1]*Department of Chemistry, Fatih University, Istanbul, Turkey*
[2]*TUBITAK-UME, National Metrology Institute, Gebze-Kocaeli, Turkey*
[3]*Department of Functional Materials, Royal Institute of Technology, Kista, Stockholm, Sweden*
[4]*Department of Materials Science and Engineering, Yildirim Beyazit University, Ulus-Ankara, Turkey*

Ba-M- and Sr-M-type hexagonal ferrites have been prepared via a sol–gel route, and the effects of adding different amounts of polyvinyl pyrrolidone (PVP) into the sol solutions. The average crystallite, size, D and σ, was obtained as for Z13 = 22 ± 2 nm and Z13-2 = 16 ± 3 nm and for Z16 = 18 ± 7 nm and Z16-2 = 17 ± 5 nm by XRD. FT-IR and TG analysis were used to prove the presence of PVP on $BaFe_{12}O_{19}$ and $SrFe_{12}O_{19}$. Based on the TGA curves the mass losses of the samples are assessed as follows: Z13 ∼15%, Z13-2 ∼25%, Z16 ∼5%, and Z16-2 ∼10%.

Keywords hexaferrites, magnetic nanomaterials, magnetization, SEM, XRD

INTRODUCTION

Hard ferrites are ceramic materials that have hexagonal crystal structure. Their formula composition can be represented as $n(MeO).m(Fe_2O_3)$, where n and m are natural numbers and Me is a divalent metal. For $n = 1$ and $m = 6$ the formula for the M-type ferrites, $MeO{\cdot}6(Fe_2O_3)$, which can also be written as $MeFe_{12}O_{19}$, is obtained. The most common M-type ferrites are those where Me is Ba, Sr, or Pb. The M-type ferrites crystallize in the magneto-plumbite structure characterized by close packing of oxygen and Me ions with iron atoms at the interstitial positions. The structure can be described as consisting of cubic blocks with the spinel structure and hexagonal blocks containing the Me ions. There are two formula units $MeFe_{12}O_{19}$ per unit cell and the Fe^{3+} ions are distributed over five nonequivalent crystallographic positions. The hard magnetic properties of hexaferrites originate from their comparatively large magnetocrystalline anisotropy, high Curie temperature, high coercive force, and high magnetic anisotropy field. Because of these properties hard ferrites still play a dominant role in the permanent magnet market owing to the low price per unit of available energy and the wide availability of the raw materials.[1]

M-type strontium ($SrFe_{12}O_{19}$) and barium ($BaFe_{12}O_{19}$) hexagonal ferrites with dimensions in nanometers have been considered as a promising material for various applications, its magnetic and morphological characteristics are extremely advantageous for a perpendicular magnetic recording medium and microwave devices.[2] By preparing tapes,[3] hard discs[4,5] and flexible or floppy discs[6] with highly oriented particles, it has been possible to obtain storage densities significantly higher than with other recording media.[7] During the search for better magnetic properties, various techniques have been developed to get single domain ferrite particles in the last decades. Aerosol pyrolysis,[8] chemical coprecipitation,[9] hydrothermal reaction,[10] sol–gel,[11] oxidation technique using nitric acid (HNO_3),[12] and self-propagating high-temperature synthesis,[13] glass crystallization,[14] microemulsion,[15] citrate precursor,[16] and salt-melt methods[17] are some examples. However, a number of difficulties in obtaining high-purity, ultra-fine, and homogeneous particles of ferrite materials with narrow size distribution have been pointed out by several investigators. To synthesize single-domain hexaferrites having high saturation magnetization together with high coercivity optimal Fe/Ba(Sr) ratio, calcination temperature, doping concentration (if there is), and other synthetic parameters should be optimized.[18] The classical ceramic method for preparing hexaferrites requires a high calcination temperature (∼1200°C), which induces sintering and aggregation on the particles. Therefore, this route is generally not preferred when size control is required.

Wet chemical synthesis through gel-to-crystallite (G-C) conversion of ultrafine ceramic powders continues to be a subject of intense research activity as these products exhibit advantages over powders derived from conventional ceramic routes. The preparation of multicomponent ceramic oxides has been well studied by the G-C conversion method.[19] The general reaction involved in this technique is the direct conversion of gel into crystallites under wet-chemical conditions, by the breakdown of

---

Received 23 September 2011; accepted 6 January 2012.

The authors are thankful to the Fatih University Research Project Foundation (Contract no: P50020902-2), Turkish Ministry of Industry, and TUBITAK (Contract no: 110T487) for financial support of this study.

Address correspondence to Z. Durmus, Department of Chemistry Fatih University, 34500, B. Cekmece-Istanbul, Turkey. E-mail: zhrdurmus@gmail.com

the gel network caused by the change in ionic pressure brought about by the chemical influx of ions.[20,21] The main advantages of this method are the increased homogeneity and high surface area of resulting powders, which lead to relatively high reactivity and hence low sintering temperatures. Furthermore, the raw materials are not expensive, making this method advantageous in terms of operational cost and procedural simplicity.

Polyvinyl pyrrolidone (PVP) deserves a special attention because of its good electrical properties, easy processability, moderate electrical conductivity, and charge transport mechanism.[22] PVP is an amorphous polymer and possesses high Tg due to the presence of the rigid pyrolidone group, which is known to form various complexes with many inorganic salts.[23]

In this study, the effects of adding different amounts of PVP into the sol solutions on the morphology of ferrite particles and their magnetic properties have been studied. To our best knowledge we present on the synthesis and detailed physicochemical characterization of this PVP/Ba-Sr hexaferrite composite materials.

EXPERIMENTAL

Instrumentation

X-ray powder diffraction (XRD) analysis was conducted on a Rigaku Smart Lab (Japan) operated at 40 kV and 35 mA using Cu K_α radiation ($\lambda = 1.54059$Å).

Fourier transform infrared (FT-IR) spectra of the samples were recorded with a Perkin-Elmer BX FT-IR infrared spectrometer (USA) in the range of 4000–400 cm^{-1}.

Scanning electron microscopy (SEM) analysis was performed, in order to investigate microstructure of samples, using Field Emission Gun JEOL 6335F (Japan). Samples were coated with gold at 10 mA for 2 min prior to SEM analysis.

The thermal stability was determined by thermogravimetric analysis (TGA; Perkin Elmer Instruments model, STA 6000, USA). The TGA thermograms were recorded for 5 mg of powder sample at a heating rate of 10°C/min in the temperature range of 30–750°C under nitrogen atmosphere.

VSM measurements were performed by using a vibrating sample magnetometer (LDJ Electronics Inc., Model 9600, USA) and magnetization measurements were carried out in an external field up to 15 kOe at room temperature.

Isothermal remanence curves were measured by applying small dc field to the sample and, then, remanent magnetization was measured after the removal of the field. The field was slightly increased to higher value and the process repeated until the sample reached the saturation remanent magnetization (M_r).

In order to measure dc demagnetization remanence, the sample was initially saturated in some direction and then field was removed to measure $M_d(H = 0)$. A small field in opposite direction was applied and removed. The remanent magnetization was measured M_d (H_1). A slightly larger opposite field was applied and removed to measure M_d (H_2, $H_2 > H_1$). This was repeated until the sample reached to saturation in opposite direction.

Procedure

The starting materials, iron (III) nitrate nonahydrate ($Fe(NO_3)_3 \cdot 9H_2O$), barium nitrate ($Ba(NO_3)_2$), strontium nitrate ($Sr(NO_3)_2$), sodium hydroxide (NaOH), citric acid ($C_6H_8O_7.H_2O$), and PVP (polyvinyl pyrrolidone) purchased from Merck (Germany), and all were of analytical purity. Stoichiometric amounts of $Fe(NO_3)_3 \cdot 9H_2O$ and $Ba(NO_3)_2$ were dissolved in a small amount of deionized H_2O by stirring at 50°C with Fe/Ba ratio of 12:1. Citric acid was then added to the mixture solution of Ba^{2+} and Fe^{3+} to chelate these ions. The molar ratios of citric acid to metal ions used were 1:1. Ammonia was added to adjust the pH value to 7. The final solution was stirred magnetically at 65°C for 2 h. The solution was then divided into two parts, and 2 g PVP and 4 g PVP were added separately to order to study the effects of PVP on the magnetic properties of Ba-hexaferrites.

All these steps were repeated with the starting materials of $Fe(NO_3)_3 \cdot 9H_2O$ and $Sr(NO_3)_2$ for the synthesis of $SrFe_{12}O_{19}$. This solution was also divided into two parts into which 2 g PVP and 4 g PVP were added separately.

Then 2 g and 4 g PVP containing (Ba-Sr) metal-citrate solutions were slowly evaporated at 80°C under constant stirring until a viscous gel was formed. By increasing the temperature up to 200°C, the gel precursors were combusted to form brown loose powders (Z13, Z13-2 precursor for Ba and Z16, Z16-2 precursor for Sr sample). Then obtained powders were calcined at 1100°C for 2 h. The hexaferrite particles were thus obtained (Z13-2 for Ba sample and Z16-2 for Sr sample). Detailed nomenclature of the materials and compositions at various processing stages are given in Table 1.

TABLE 1
Nomenclature of the products

Sample name	Z13 precursor	Z13	Z13-2 precursor	Z13-2	Z16 precursor	Z16	Z16-2 precursor	Z16-2
Composition	$BaFe_{12}O_{19}$				$SrFe_{12}O_{19}$			
Amount of PVP	2 g	2 g	4 g	4 g	2 g	2 g	4 g	4 g
Calcined (1100°C for 1 h)	No	Yes	No	Yes	No	Yes	No	Yes

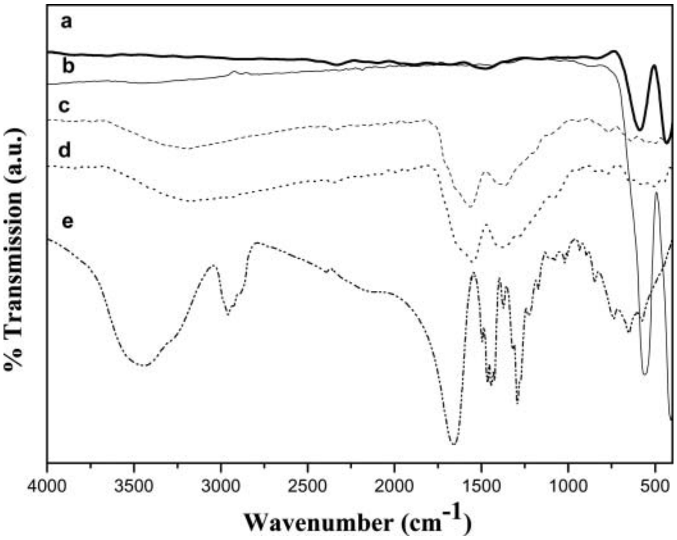

FIG. 1. FT-IR spectra of (a) Z13-2, (b) Z13, (c) Z13 precursor, (d) Z13-2 precursor, and (e) PVP.

RESULTS AND DISCUSSION

FT-IR Analysis

FT-IR spectra of Ba and Sr hexaferrites are presented in Figures 1 and 2, respectively. In the FT-IR spectra of calcined samples of Z13, Z13-2, Z16, and Z16-2 there are typical bands for ferrites observed. In the spectrum for pure PVP (Figure 1; C=O stretch band is present at 1660 cm^{-1} and after formation of PVP–nitrate complex (precursor samples of Z13, Z13-2, Z16, Z16-2) this stretching shifts ~20 cm^{-1}, indicating a strong interaction between nitrates and C=O of PVP host matrix.[24] The asymmetric CH$_2$ stretch (2952 cm^{-1}) and symmetric CH$_2$ stretch (2892 cm^{-1}) shifted to 2922 and 2852 cm^{-1}, respectively.[25] From the curve (Figure 2), it can be seen the adsorption bands at around 420, 543, and 584 cm^{-1} correspond to typical M-O adsorption bands in BaFe$_{12}$O$_{19}$ and SrFe$_{12}$O$_{19}$.

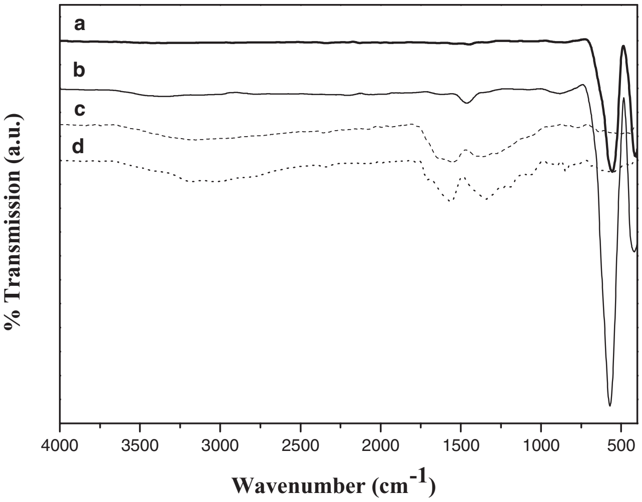

FIG. 2. FT-IR spectra of **a)** Z16-2, **b)** Z16, **c)** Z16 precursor and **d)** Z16-2 precursor.

XRD Analysis

Phase investigation of the crystallized products BaFe$_{12}$O$_{19}$ and SrFe$_{12}$O$_{19}$ were performed by XRD and the diffraction patterns are presented in Figures 3 and 4, respectively. The XRD powder patterns indicate that the products are M-type BaFe$_{12}$O$_{19}$/SrFe$_{12}$O$_{19}$ and the diffraction peaks are broadened owing to very small crystallite size. All of the observed diffraction peaks are indexed, as presented, by the hexagonal structure of BaFe$_{12}$O$_{19}$/SrFe$_{12}$O$_{19}$, revealing a high phase purity of hexaferrite agreeing with those reported for Ba-hexaferrite (JCPDS card number 84–0757) and for Sr-hexaferrite (JCPDS card number 84–1531) including minor phase Fe$_2$O$_3$ with card number 76–1821.[26,27] The mean size of the crystallites was estimated from the diffraction pattern using the line profile fitting equation given in Wejrzanowski et al.[28] and Pielaszek.[29] The line profiles, shown in Figure 3 were fitted for observed 24 peaks for Z13 and 25 peaks for Z13-2 samples with the following Miller indices: (002), (102), (006), (105), (106), (110), (008), (107), (114), (200), (108), (203), (205), (206), (118), (207), (1011), (213), (209), (300), (303), (1112), (218), (1014), (220), (1114), (2014), and (311). The average crystallite, size, D and σ, was obtained as for Z13 = 22 ± 2 nm and Z13-2 = 16 ± 3 nm as a result of this line profile fitting.

The line profiles, shown in Figure 4 for SrFe$_{12}$O$_{19}$ were fitted for observed 24 and 25 peaks for Z16 and Z16-2 samples with the following Miller indices: (100), (102), (006), (105), (106), (110), (008), (112), (107), (114), (201), (203), (116), (109), (205), (206), (207), (1011), (209), (2010), (217), (2011), (1112), (220), (309), (2111), (2014), and (2112). The average crystallite, size, D and σ, was obtained as for Z16 = 18 ± 7 nm and Z16-2 = 17 ± 5 nm as a result of this line profile fitting.

Magnetization Measurements

Room temperature magnetization curves of PVP modified barium (BaFe$_{12}$O$_{19}$) and strontium (SrFe$_{12}$O$_{19}$) hexaferrites are shown in Figure 5. The M-H hysteresis curve of Z13 does not reach to a saturation up to 15 kOe, which indicates that they are within the single domain limit (i.e., particle size $< 1\ \mu$m). The specific saturation magnetization of the Z13 sample is around 65 emu/g that is close to the theoretical value of this hexaferrite (i.e., 72 emu/g) and that of Z13-2 are ~54 emu/g. The coercive fields of the samples, which depends on the particle size very much, are quite high that is 5.1 and 6 kOe for the Z13 and Z13-2, respectively. We can state that our samples mainly consist of fine Ba-M particles because coercive field increases with decreasing particle size.

The squareness ratio, Mr/Ms, for the Z13 and Z13-2 is around 0.55, which also indicates that particles are within the single domain limit. This is clearly shown in the SEM micrographs presented in Figure 9, which reveals that average particle size is around 250 nm and it is possible to see particles as small

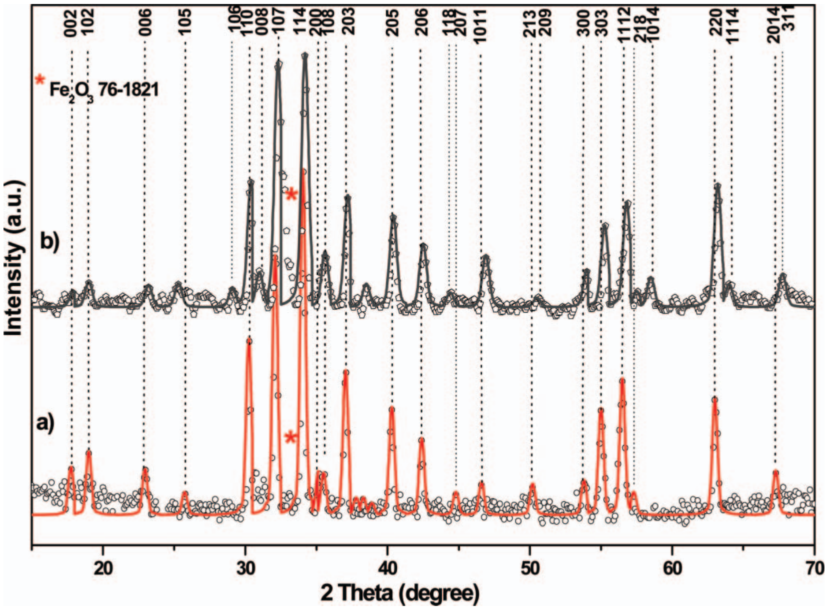

FIG. 3. XRD patterns and line profile fitting of (a) Z13 and (b) Z13-2 (color figure available online).

as 30 nm. Like $BaFe_{12}O_{19}$, both Z16 and Z16-2 $SrFe_{12}O_{19}$ nanoparticles also have unsaturated specific magnetization revealing the fine particle structure of the samples. The coercive field of the Z16 sample is 5 kOe and decreases to 3.6 kOe in the Z16-2, see Table 2.

The M-H hysteresis curve of the Z16-2 is "bee waist" type, indicating that magnetic interactions in this sample differs from that of the Z16. To interpret this type of magnetization curve, we first should mention the spin states in hexaferrites. They have hexagonal symmetry with space group P63/mmc and 64 ions per cell located in 11 distinct basis sites. The 24 Fe^{3+} atoms are placed on three octahedral sites (12k, 2a, and 4f2),

TABLE 2
The magnetic parameters of Z13, Z13-2, Z16, and Z16-2 samples

	$BaFe_{12}O_{19}$		$SrFe_{12}O_{19}$	
	Z13	Z13-2	Z16	Z16-2
M_s, emu/g	64.7	54.5	61.5	57.6
M_r, emu/g	35.5	29.9	33.7	32.8
M_r/M_s	0.55	0.55	0.55	0.57
H_c, kOe	5.1	6	3.6	5

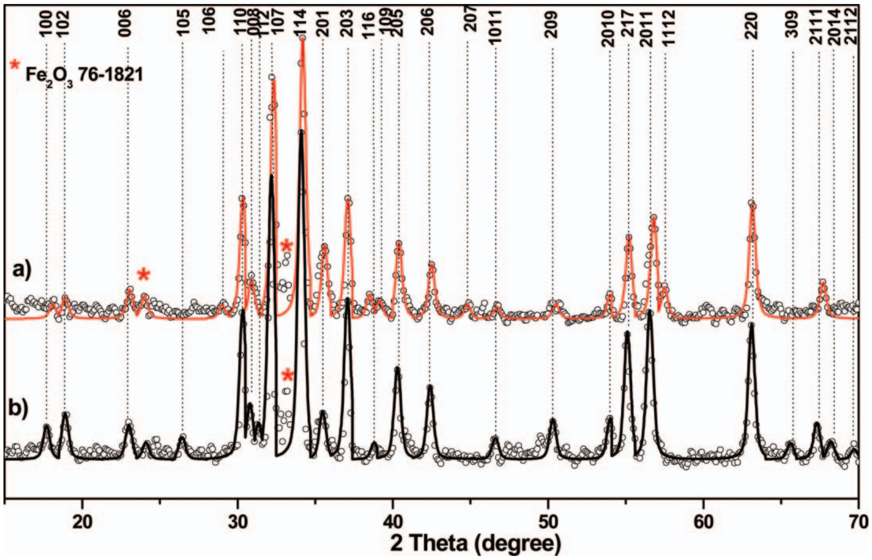

FIG. 4. XRD patterns and line profile fitting of (a) Z16 and (b) Z16-2 (color figure available online).

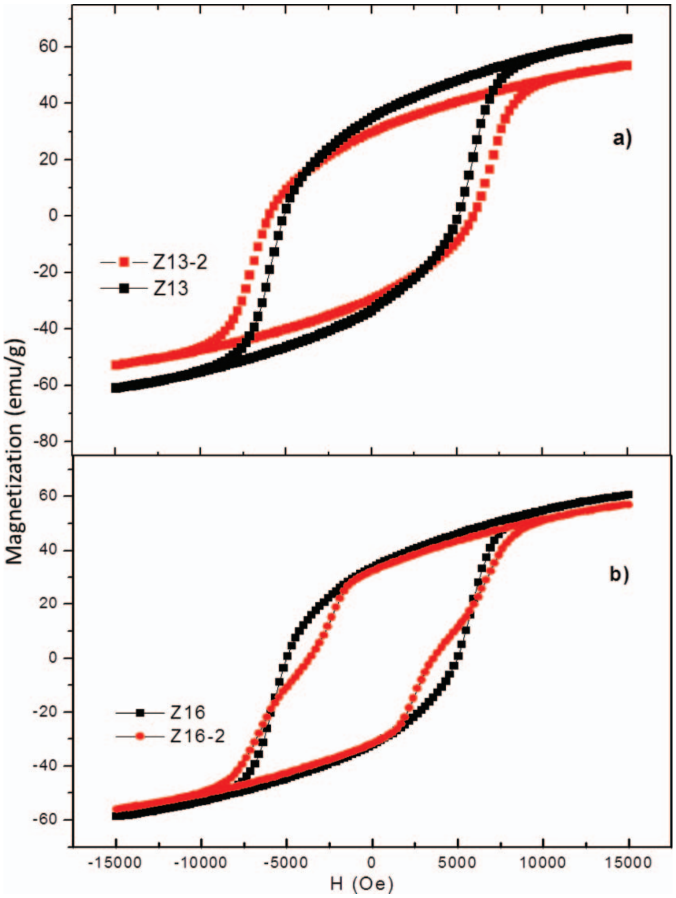

FIG. 5. M versus H curves at room temperature (a) Z13 and Z13-2 and (b) Z16 and Z16-2 samples, deduced from the Stoner–Wohlfarth model (color figure available online).

one tetrahedral site (4f1) and one trigonal bipyramidal site (2b). The spins in the 12k-, 2a-, and 2b-sites are parallel to each other and to the crystallographic *c*-axis, whereas those in 4f2 and 4f1 point in the opposite direction. Their mutual orientation is given by the Gorter collinear model as 12k (↑), 4f1 (↓), 4f2 (↓), 2a (↑), and 2b (↑). Ferro- and antiferromagnetically ordered sites are coupled by the super exchange interactions through the O_2 atoms. The net magnetic polarization J at a temperature T per formula unit (f.u.) can be expressed as:

$$\begin{aligned} J(T) = 6m_{12k}(T) - 2m_{4f1}(T) - 2m_{4f2}(T) \\ + 1m_{2a}(T) + 1m_{2b}(T) \end{aligned} \qquad [1]$$

where m_n describes the magnetic moment of Fe^{3+} ion in the *n*th sublattice. The Stoner–Wohlfarth model[30] describes the way to understand type of magnetic interactions between these spin states, magnetizing- or demagnetizing-like, at a particular magnetic field, H, by measuring two principal remanence curves M_r and M_d. They are related by the following equation:

$$M_d(H)/M_r(\infty) = 1 - 2M_r(H)/M_r(\infty) + \delta M(H) \qquad [2]$$

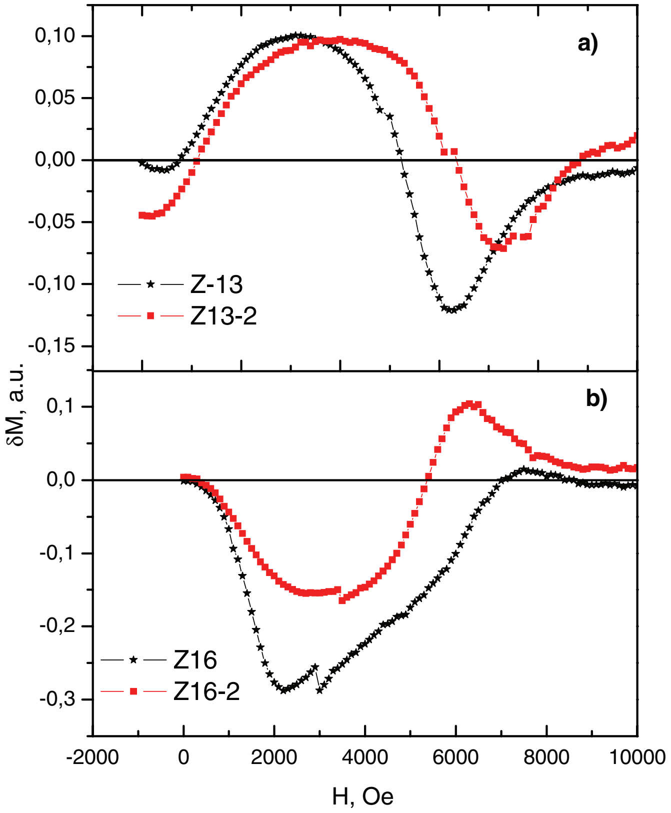

FIG. 6. Magnetic interactions of **a)** Z13 and Z13-2 and **b)** Z16 and Z16-2 samples, deduced from the Stoner–Wohlfarth model (color figure available online).

where $\delta M(H)$ is the interaction term and $M_r(\infty)$ describes the saturation value of the isothermal remanence. For non-interacting systems, this plot shows a horizontal line through the origin. Positive (negative) values of $\delta M(H)$ correspond to

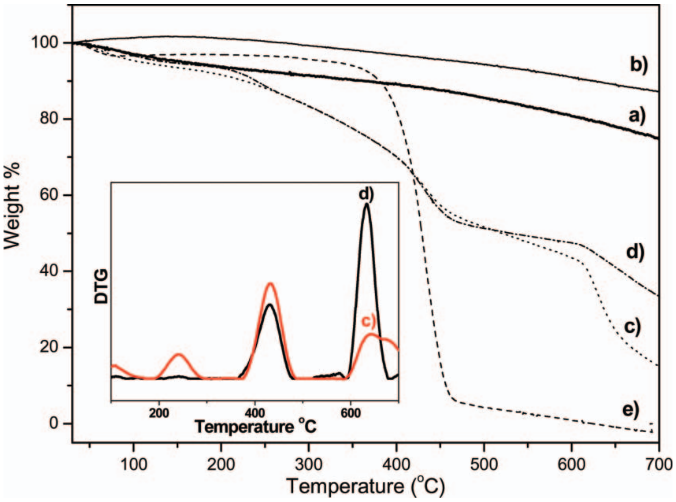

FIG. 7. TGA thermograms of (a) Z13-2, (b) Z13, (c) Z13-2 precursor, (d) Z13 precursor, and (e) PVP (color figure available online).

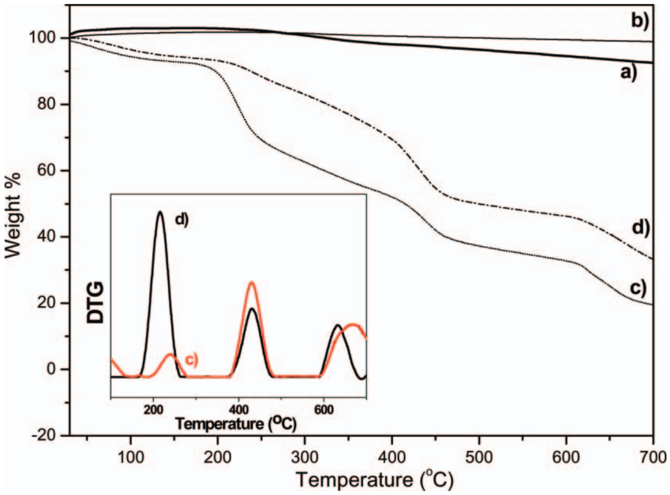

FIG. 8. TGA thermograms of (a) Z16-2, (b) Z16, (c) Z16-2 precursor, and (d) Z16 precursor (color figure available online).

the magnetizing-like (demagnetizing-like) interactions. Figure 6 shows the magnetic interactions in samples of $BaFe_{12}O_{19}$ and $SrFe_{12}O_{19}$. In Z13, $BaFe_{12}O_{19}$ sample, magnetizing-like interactions appear in 0.7 and 5.1 kOe range and demagnetizing-like interactions becomes dominant at higher fields. In the Z13-2, field range of both interaction types is shifted to higher magnetic fields. For instance, constructive interactions (i.e., magnetizing-like) appears between 1 kOe and 6 kOe and above spins states interact destructively to destabilize the remanence state. However, strength of destructive interactions decreases by coating. In Z16, $SrFe_{12}O_{19}$ sample, a demagnetizing-like interaction appears in the whole field range. For Z16-2, profile of the $\delta M(H)$ curve shows different contributions of exchange interactions. The strength of demagnetizing-like interactions decreases and surprisingly magnetizing-like interactions appears around 5 kOe most probably due to the pinning (i.e., cancellation) of some spin states at 4f1 and/or 4f2 sites that are used in superexchange interactions between the Fe^{3+} ions. We think that the reason of "bee waist" type magnetization is probably due to this magnetizing-like interaction above 5 kOe.

TG Analysis

Thermal stability and decomposition characteristic of samples were evaluated by TGA analysis and thermograms for sample series Z13 and Z16 are presented in Figures 7 and 8, respectively. The thermal behavior of Z13-2 and Z13 samples are more or less same (Figure 7). The observed weight loss of Z13-2 sample (Figure 7) is much more than that of Z13 sample (Figure 7) due its high content of PVP. In Figure 7, the first step was the dehydration of adsorbed water. In second step, the exothermic peak at about 265°C for the Z13 precursor and Z13-2 precursor

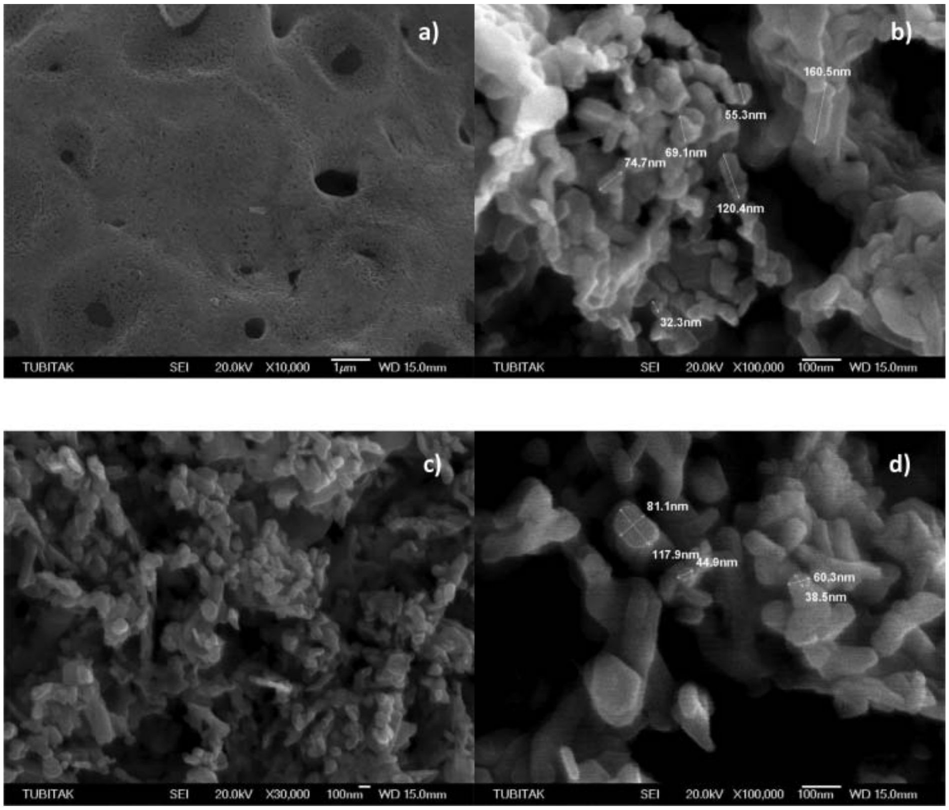

FIG. 9. SEM micrographs of sample Z13 (a, b) and Z13-2 (c, d) at different magnifications.

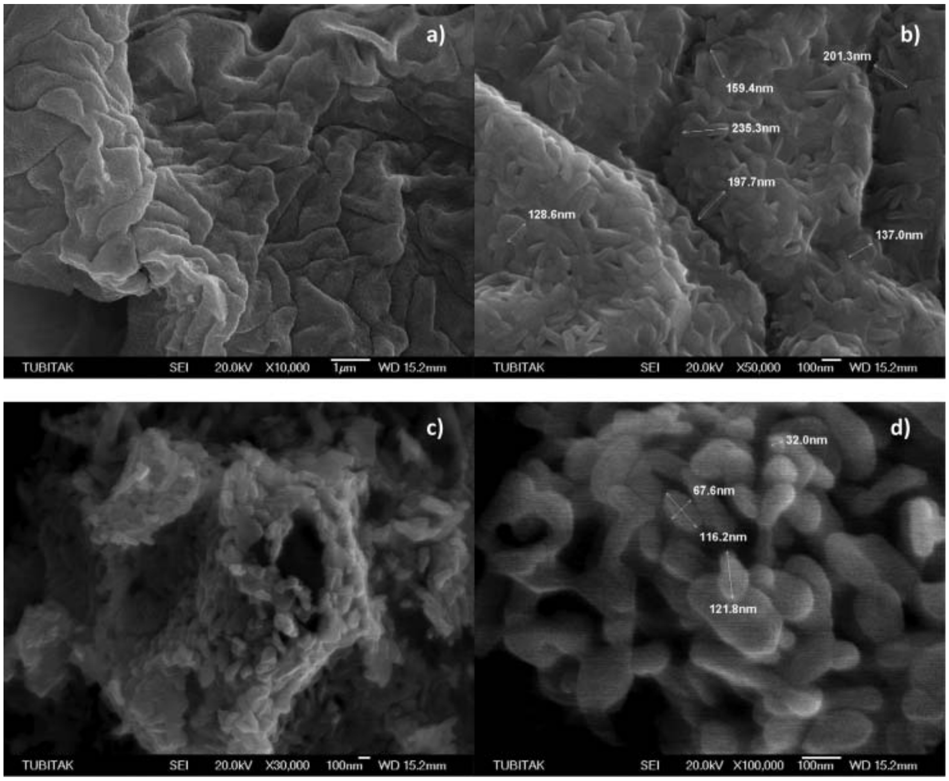

FIG. 10. SEM micrographs of sample Z16 (a, b) and Z16-2 (c, d) at different magnifications.

may be attributed to the decomposition of organic salts including iron citrate and barium acetate along with the degradation of PVP through the intermolecular cross-linking reaction[29–31] and this degradation is more intense in Figure 7 (due to the presence high amount PVP in Z13-2 precursor sample). The third step at around 315–470°C involves 30% weight loss and accompanies two sharp exothermic peaks at 400 and 429°C, which could be attributed to the oxidation of carbon released by the decomposition of PVP.[32]

Thermograms (Figure 7) did not reach a plateau within the measurement temperature range. Samples were then taken and calcined at 900°C in order to determine the percentage of organic and inorganic constituents. Thermogram of PVP (Figure 7) reached the plateau at 700°C. As it seen in Figure 8, similar thermal behaviors were also observed for the $SrFe_{12}O_{19}$ sample.

Based on the losses the inorganic content of the samples are assessed as follows: Z13 ∼15%, Z13-2 ∼25%, Z16 ∼5%, and Z16-2 ∼10%.

SEM Analysis

SEM micrographs of samples Z13, Z13-2, Z16, and Z16-2 are presented in Figures 9 and 10. In all of the micrographs very small particles are visible, however, due to the combustion process at elevated temperatures there is strong necking/sintering observed. General view of the surfaces is like a sintered body and observed pores are formed due to the quick escape of gases formed at high temperature treatment, during the decomposition of organic matter. Looking at the samples at higher magnification, grains as large as ∼400 nm and some free particles as small as ∼30 nm were observed for all samples. It is hard to understand the effect of increasing concentration of PVP in the final morphology/microstructure of the materials due to the extensive sintering. It is also worth to mention that the crystallite size estimated from X-ray line profile fitting is smaller than the observed grains/particles, which reveal polycrystalline nature of the synthesized hexaferrite nanomaterials.

CONCLUSION

M-type hexagonal ferrites ($BaFe_{12}O_{19}$) and $SrFe_{12}O_{19}$) have been prepared using the sol–gel synthesis technique, and their magnetic properties and morphologies were investigated for the different preparation conditions: Two samples were prepared with the addition of 2 g and 4 g PVP into the sol solutions of Ba and Sr, respectively. The ferrites prepared with more PVP added have lower coercivity. Our results indicate that adding PVP 2000 into the sol solution can be an effective way to tune the magnetic properties of M-type hexagonal ferrites.

REFERENCES

1. Buschow, K.H.J. *Concise Encyclopedia of Magnetic & Superconducting Materials,* 2nd ed.; Oxford, England: Elsevier, **1992**.

2. Wohlfarth, E.P. *Ferromagnetic Materials: A Handbook on the Properties of Magnetically Ordered Substances*; Amsterdam, the Netherlands: North-Holland, Elsevier, **1982**.
3. Yamamori, K.; Tanaka, T.; Jitosho, T. *IEEE Trans. Magn.* **1991**, *27*, 4960.
4. Speliotis, D.E. *J. Appl. Phys.* **1987**, *61*, 3878.
5. Speliotis, D.E. *IEEE Trans. Mag.* **1987**, *23*, 25.
6. Fujiwara, T.; Issiki, M.; Koike, Y.; Oguchi, T. *IEEE Trans. Magn.* **1982**, *18*, 1200.
7. Valenzuela, R. *Magnetic Ceramics*; Cambridge, England: Cambridge University Press, **1994**.
8. Tang, Z.X.; Nafis, S.; Sorensen, C.M.; Hadjipanayis, G.C. *IEEE Trans. Magn.* **1989**, *25*, 4236.
9. Janasi, S.R.; Emura, M.; Landgraf, F.J.; Rodrigues, D.J. *IEEE Trans. Magn.* **2000**, *36*, 3327.
10. Barb, D.; Diamandescu, L.; Rusi, A.; Tarabasanu-Mihaila, D.; Morariu, M.; Teodorescu, V. *J. Mater. Sci.* **1986**, *21*, 1118.
11. Zhong, W.; Ding, W.; Zhang, N.; Hong, J.; Yan, Q.; Du, Y. *J. Magn. Magn. Mater.* **1997**, *168*, 196.
12. Sozeri, H. *J. Magn. Magn. Mater.* **2009**, *321*, 2717.
13. Affleck, L.; Aguas, M.D.; Parkin, I.P.; Pankhurst, Q.A.; Kuznetsov, M.V. *J. Mater. Chem.* **2000**, *10*, 1925.
14. Rezlescu, L.; Rezlescu, E.; Popar, P.D.; Rezlescu, N. *J. Magn. Magn. Mater.* **1993**, *193*, 288.
15. Liu, X.; Wang, J.; Gan, L.M.; Ding, S.C.; Ng, J. *J. Magn. Magn. Mater.* **1998**, *184*, 344.
16. Sankaranarayanan, V.K.; Khan, D.C. *J. Magn. Magn. Mater.* **1996**, *153*, 337.
17. Chin, T.S.; Hsu, S.L.; Deng, M.C. *J. Magn. Magn. Mater.* **1993**, *120*, 64.
18. Sözeri, H.; Küçük, İ.; Özkan, H. *J. Magn. Magn. Mater.* **2011**, *323*, 1799.
19. Padmini, P.; Kutty, T.R. N. *J. Mater. Chem.* **1994**, *4*, 1875.
20. Kutty, T.R. N.; Padmini, P. *Mater. Res. Bull.* **1992**, *27*, 945.
21. Diaz-Guemes, M.I.; Carreno, T.G.; Serna, C.J.; Palacios, J.M. *J. Mater. Sci.* **1989**, *24*, 1011.
22. Armand, M.B.; Chabagno, J.M.; Duclot, M. International Conference on Solid Electrolytes, University of St Andrews, Scotland, **1988**.
23. Ulański, J.; Polanowski, P.; Tracz, A.; Hofmann, M.; Dormann, E.; Laukhina, E. *Synth. Met.* **1998**, *94*, 23.
24. Baykal, A.; Bıtrak, N.; Unal, B.; Kavas, H.; Durmus, Z.; Ozden, S.; Toprak, M.S. *J. Alloys Compd.* **2010**, *502*, 199.
25. Kong, S.; Zhang, P.; Wen, X.; Pi, P.; Cheng, J.; Yang, Z.; Hai, J. *Particuol.* **2008**, *6*, 185.
26. Mou, F.; Guan, J.; Sun, Z.; Fan, X.; Tong, G. *J. Solid State Chem.* **2010**, *183*, 736.
27. Han, M.; Ou, Y.; Chen, W.; Deng, L. *J. Alloys Compd.* **2009**, *474*, 185.
28. Wejrzanowski, T.; Pielaszek, R.; Opaliniska, A.; Matysiak, H.; Lojkowski, W.; Kurzydlowski, K. *J. Appl. Surf. Sci.* **2006**, *253*, 204.
29. Pielaszek, R. Analytical expression for diffraction line profile for polydispersive powders. In *Applied Crystallography: Proceedings of the XIX Conference*, Krakow, Poland **2003**, 43.
30. Remiro, P.M.; Cortazar, M.M.; Calahorra, M.E. *J. Mater. Sci.* **1999**, *34*, 2627.
31. Wang, Z.L.; Liu, X.J.; Chai, M.F.; Lv, P.; Liu, Y.; Meng, J. *J. Phys. Chem. B.* **2008**, *112*, 11292.
32. Wohlfarth, E.P. *J Appl. Phys.* **1958**, *29*, 595.